PALSAR Multi-Mode Interferometric Processing

Charles Werner, Urs Wegmüller, Tazio Strozzi, Andreas Wiesmann, and Maurizio Santoro

Gamma Remote Sensing, Worbstrasse 225, CH-3073 Gümligen, Switzerland,
Email: cw@gamma-rs.ch

Abstract

The main objective of the project "ALOS PALSAR quality assessment, calibration, and validation research" (ALOS-RA-175) is to independently validate PALSAR data for applications focusing specifically on interferometry. As development platform we have developed an independent processing chain (GAMMA) that takes into account the specific features of the PALSAR instrument and data characteristics.

In a first part the PALSAR data characteristics and the raw data processing we performed are discussed. In a second part we describe the processing techniques used to generate interferograms between single and dual polarization PALSAR data sets.

1. PALSAR RAW DATA CHARACTERISTICS AND SAR PROCESSING

1.1. PALSAR raw data characteristics

For PALSAR fine-beam single-polarization mode (HH) acquisitions we found characteristics as shown in Table 1. The Doppler spectrum at the center of the swath, modulo the SAR pulse repetition frequency is shown in Figure 1. The Doppler ambiguity was resolved using the multi-look beat frequency (MLBF) algorithm as described by Cumming and Wong [2]. The Doppler centroid as a function of range was estimated by cross-correlation of adjacent lines and is shown in Figure 2. It is important to notice that such high Doppler Centroid values and significant range dependence of the Doppler Centroid was only observed during the initial phase. Later on zero-Doppler steering was applied very successfully, so that the Doppler Centroids determined were all close to zero.

Table 1   ALOS PALSAR Fine-Beam raw data characteristics.

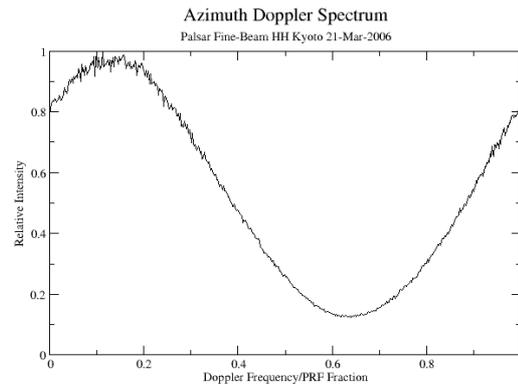|	
Radar Center Frequency:	1270.000 MHz
Polarization	HH
Range Bandwidth	28.000 MHz
Chirp Duration	27 micro-sec.
Range Sample rate (IQ)	32.000 MHz
Number of range samples/echo	10304
Number of echoes	32421
Number of bits/sample	5
Pulse Repetition Frequency (PRF)	2159.827 Hz

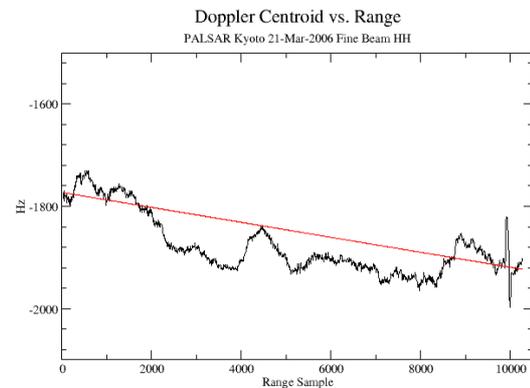*Figure 1. Azimuth spectrum at center-swath, modulo the SAR Pulse Repetition Frequency*

Figure 2. Doppler versus slant-range sample number (for a data set acquired early on before operation with zero Doppler steering).

1.2. SAR processing

Level-1 complex signal samples were processed using the Gamma MSP to produce single-look complex (SLC) and multi-look intensity (MLI) images. In fine-beam mode the transmit chirp is 28 MHz and lasts 27 micro-seconds.

The data were processed using a range-Doppler algorithm including secondary range migration. Autofocus confirmed that the effective along-track velocity determined from the state vectors was accurate at the level of .5 m/s. The antenna pattern provided are used for the radiometric calibration. A small section of a very early image processed with MSP showing the full range resolution and 3 azimuth looks is shown in Figure

3. Note the individual roads and buildings visible in the scene. For the 1 range x 3 azimuth looks MLI an equivalent number of looks (ENL) of 2.3 to 2.5 was determined. Radio-Frequency-Interference (RFI) filtering is applied.

Figure 3. Full range resolution section of the PALSAR Kyoto image acquired on 21-Mar-2006. The slant range sampling corresponds to an approx. ground range sampling of 7.9 m, the azimuth pixel spacing (3-look) is 9.55 m.

1.3. PALSAR Processing Point Target Response

In the processed SLC further analysis was performed to evaluate the point target performance in the image. A bright target was selected in the center of the image and analyzed using the Gamma point target analysis program to evaluate range and azimuth resolution, peak and integrated sidelobe levels and phase characteristic. Plots of range and azimuth cuts of the point target response are shown in Figures 4 and 5. Peak and integrated sidelobe levels are summarized in Table 2.
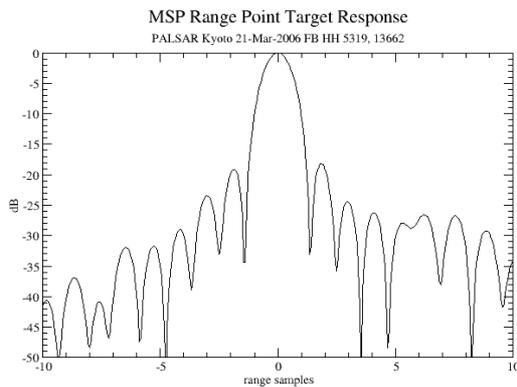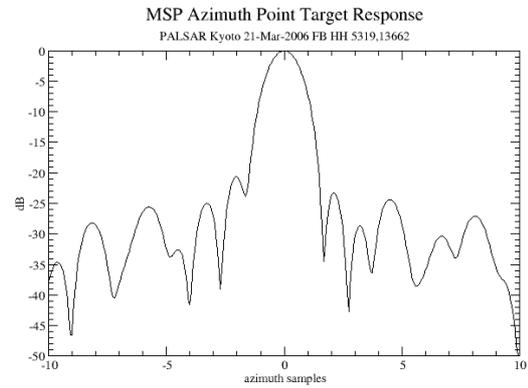

Figure 4. Point target response in range.

Figure 5. Point target response in azimuth.

Table 2. Point target resolution, peak side-lobe, and integrated side-lobe levels in range and azimuth.

range -3 dB width (samples):	1.188
range -10 dB width (samples):	1.996
range PSLR (dB):	-16.787
range ISLR (dB):	-16.851
azimuth -3 dB width (samples):	1.371
azimuth -10 dB width (samples):	2.332
azimuth PSLR (dB):	-20.661
azimuth ISLR (dB):	-18.247

2. PALSAR MULTI-MODE INTERFEROMETRIC PROCESSING

2.1. Introduction

The number of PALSAR data acquisition modes has been restricted to simplify mission planning and acquire a uniform archive that will maximize the utility of the data for different users. The primary data acquisition modes during ascending passes are Fine-Beam Single (FBS) and Fine-Beam Dual (FBD). In FBD dual polarization data (HH- and HV-polarization) are acquired. Since October 2006, the FBS and FBD data are both acquired with an off-nadir angle of 34.3 deg. The FBD data at HH polarization are acquired using half the range bandwidth of the FBS data, i.e. 14 MHz instead of 28 MHz. The center frequency is the same and so the range bands fully overlap permitting interferometric processing of mixed FBS – FBD pairs.

We describe in the following the processing technique applied to generate interferograms between FBS and FBD data. The ability to do this greatly increases the interferometric monitoring capability of PALSAR.

2.2. FBS – FBD interferogram generation

In a first step each scene is processed individually using the appropriate chirp and sampling rates. Then a range over-sampling by a factor two is applied to the FBD scene to transform it to the same sample spacing as the FBS scene. Then the FBS SLC and the oversampled FBD scene are co-registered to a common reference geometry. Then we apply common band filter taking into account the smaller bandwidth of the FBD scene. And finally we calculate the interferogram.

Because of the high resolution sampling rate taking into account the terrain height in the resampling may be required. We do this by generation of a lookup table that relates the two SAR image geometries. This requires a DEM in the geometry of the reference scene image and precise state vectors. For each point in the reference scene we determine the location in the DEM that is being imaged. Then we determine at what time and slant-range that point is imaged by the radar in the second track. A refinement in the lookup table is performed using a cross-correlation analysis for small image patches. This approach resamples the SLC data at better than 1/10 pixel accuracy including baseline and terrain effects. Common-band filtering between the scenes can be done slope adaptively. The radar pulse samples a small bandwidth of the spatial reflectivity spectrum of the surface. For a particular frequency f, the equivalent wavenumber k at the surface is:

$$k_x = \frac{4\pi f}{c}\sin(\theta - \xi) \quad \theta : \text{look angle} \quad \xi : \text{surface slope}$$

The second interferometer antenna records a different part of the spectrum shifted by

$$\Delta f = \frac{fB_\perp}{2r_0 \tan(\theta - \xi)} \quad B_\perp : Bperp \quad r_0 : \text{Slant Range}$$

Spectral shift filtering removes the effect of baseline decorrelation for level surfaces. There is a proportional loss of range resolution.

2.3. Example

An example of a PALSAR FBS – FBD differential interferogram over a mining area in Poland is shown in Figure 5. The locations with excavation during the period considered can clearly be identified because of the dm scale subsidence occurring above the excavation. For further discussion of other examples it is referred to [2].

3. CONCLUSIONS

PALSAR data was found to be of excellent quality and well suited for interferometry.

It was explained how PALSAR FBS and FBD acquisitions can be combined interferometrically. An example was shown demonstrating the feasibility and potential of PALSAR FBS – FBD interferometry. This possibility strongly improves INSAR opportunities as FBS and FBD acquisitions are acquired consistently at the same incidence angle.

FBS and FBD acquisitions can also be combined in offset tracking which strongly improves offset tracking opportunities.

4. ACKNOWLEDGMENTS

5. REFERENCES

[1] Cumming, I., F. Wong, Digital Processing of Synthetic Aperture Radar Data, Chapter 12, pp. 481-565, Artech House, 2005.

[2] Wegmüller U., T. Strozzi, C. Werner, A. Wiesmann, V. Spreckels, N. Benecke, and D. Walter, "Monitoring of mining induced surface deformation", Procs First joint PI Symposium of ALOS data nodes for ALOS Science Program, 19-23. Nov. 2007, Kyoto, Japan.
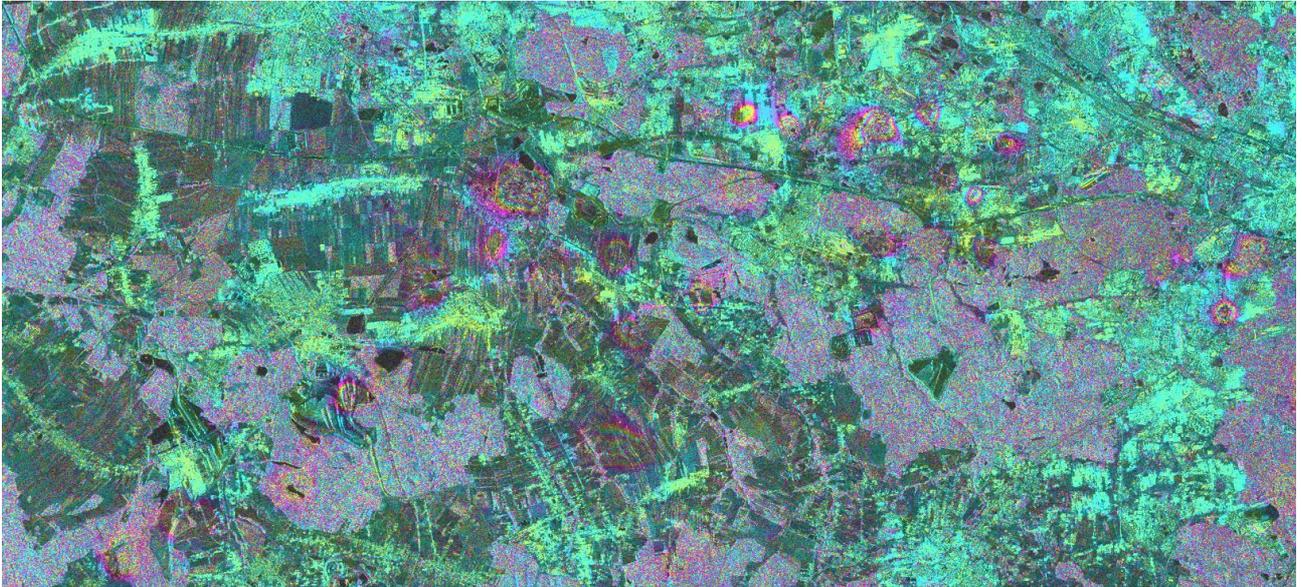
Figure 5. Section of a georeferenced PALSAR FBS – FBD differential interferogram over mining area in Poland, 20070222_20070710, Δt=138days, $B_\perp$=809m. One color cycle corresponds to 11.7cm displacement along the line-of-sight direction.